Journal of Structural Geology 97 (2017) 189–198

Contents lists available at ScienceDirect

Journal of Structural Geology

journal homepage: www.elsevier.com/locate/jsg

A new model for the computation of the formation factor of core rocks

A. Beltrán [a, *], O. Chávez [b], J. Zaldivar [c], F.A. Godínez [b, d], A. García [c], R. Zenit [e]

[a] Instituto de Investigaciones en Materiales, Unidad Morelia, Universidad Nacional Autónoma de México, Antigua Carretera a Pátzcuaro No. 8701, Col. Ex Hacienda de San José de la Huerta, 58190, Morelia, Michoacán, Mexico
[b] División de Estudios de Posgrado e Investigación, Instituto Tecnológico de Chihuahua, Av. Tecnológico No. 2909, C.P. 31310, Chihuahua, Chih., Mexico
[c] Tecnología Aplicada en Exploración y Producción Petrolera, Inc., Homero 714, Polanco, D.F. 11560, Mexico
[d] Instituto de Ingeniería, Universidad Nacional Autónoma de México, Apdo. Postal 70-360, Ciudad Universitaria, D.F. 04510, Mexico
[e] Instituto de Investigaciones en Materiales, Universidad Nacional Autónoma de México, Apdo. Postal 70-360, Ciudad Universitaria, D.F. 04510, Mexico

ARTICLE INFO

Article history:
Received 21 July 2016
Received in revised form
20 February 2017
Accepted 2 March 2017
Available online 6 March 2017

Keywords:
Formation factor
Mathematical model
Core rock lithologies
Tortuosity

ABSTRACT

Among all the rock parameters measured by modern well logging tools, the formation factor is essential because it can be used to calculate the volume of oil- and/or gas in wellsite. A new mathematical model to calculate the formation factor is analytically derived from first principles. Given the electrical properties of both rock and brine (resistivities) and tortuosity (a key parameter of the model), it is possible to calculate the dependence of the formation factor with porosity with good accuracy. When the cementation exponent ceases to remain constant with porosity; the new model is capable of capturing both: the non-linear behavior (for small porosity values) and the typical linear one in log-log plots for the formation factor vs. porosity. Comparisons with experimental data from four different conventional core rock lithologies: sands, sandstone, limestone and volcanic are shown, for all of them a good agreement is observed. This new model is robust, simple and of easy implementation for practical applications. In some cases, it could substitute Archie's law replacing its empirical nature.

1. Introduction

Oil and natural gas are considered to be the most important sources of energy in the world. In petroleum industry, well logs play a fundamental role in exploration and reservoir characterization e.g. (Egbai and Aigbogun, 2012). The primary objectives of logging in an exploration site are to locate and to quantify the amount of hydrocarbons in the vicinity of a borehole. There are many different types of well logs including gamma ray, caliper, density, neutron, sonic and electrical resistivity logs, among others e.g. (Yan, 2002). Possibly, the most important and widely studied of these is the electrical resistivity log, which is used routinely to calculate the porosity and saturation of reservoir rocks both quantities related to the interpretation and analysis of the reservoir content. Strictly speaking, the electrical resistivity log is a function of several physical parameters and lithological attributes, including electric resistivities of formation and pore water; temperature, viscosity, and degree of saturation of pore water; type and amount of clays; mechanism of charge fixation at the fluid - solid interface (represented by specific surface area and electric surface conductance); intricate geometry of pores and pore channels (i.e. tortuosity among others parameters); the ratio of the volume of voids to total volume (represented by the effective porosity); formations ability to transmit pore water (represented by permeability); cation exchange capacity; and size, shape, type (mineralogy), packing, sorting, and distribution of grains.

Typically, the study of electrical resistivity of such reservoir formations is done by saturating the rocks core with a brine solution (conducting liquid) in order to measure the electrical resistivity of this bulk system, R_0 (Sheriff, 1974). Since the resistivity of the saturating liquid is known, R_l, it is possible to calculate the formation factor defined as:

$$F = \frac{R_0}{R_l}. \tag{1}$$

Extensive experimental work has shown that the bulk resistivity of a rock, R_0, depends on its porosity, pore fluid resistivity and saturation (Waxman and Smits, 1968; Waxman, 1974; Clavier et al., 1977; Givens, 1987). Consequently, from a theoretical point of view, most of the efforts have been focused on developing mathematical relationships between water resistivity, porosity and water

* Corresponding author.
E-mail address: albem@iim.unam.mx (A. Beltrán).

http://dx.doi.org/10.1016/j.jsg.2017.03.001
0191-8141/

List of symbols

R_0	Electrical resistivity of the bulk system
R	electrical resistivity
r	symbol for the rock phase
l	symbol for the liquid phase
F	formation factor
Φ	porosity
m	cementation exponent
G	tortuosity
φ	dimensionless electrical current density
ξ	dimensionless radial coordinate
b	pore-rock system radius
r^*	dimensional radial coordinate
J	dimensional current density at any radius
J_a	dimensional current density at the pore radius
δ	skin depth parameter
ε	ratio of the skin depth parameter δ and pore size.
μ	magnetic permeability of the medium
ω	frequency of the electrical signal
β	fitting parameter
c	aspect ratio parameter
m_A	cementation exponent based on Archie's law
m_t	average cementation exponent
ΔT_c	characteristic temperature drop.
θ	dimensionless temperature
ϕ	temperature coefficient for resistivity

saturation. In a seminal work published by Archie (1942), an empirical relationship between the formation factor and porosity (Φ) for different lithologies was formulated as:

$$F = \Phi^{-m} \tag{2}$$

where the constant m is often known as the cementation exponent. The cementation exponent provides implicit information about the pore structure. Equation (2) is commonly referred to as Archie's law and it is still the most widely used expression for resistivity log interpretation. Practical applications of Archie's law in a particular area requires a knowledge of Φ and m from the laboratory measurements or studies of a well logging data in such area. Despite its prevalence and simplicity, Equation (2) is, in fact, a coarse and an oversimplified model. Its limitations are evident when contrasted with various experimental data.

The study of the formation factor constitutes in itself a classic subject of petrophysics research (Archie, 1942; Pérez-Rosales, 1982; Saner et al., 1996), since it provides a useful and convenient evaluation of the nature of the pore structure of reservoir rocks. Archie's law, according to Equation (2) states that F is a function of a power of Φ; when plotted in a log-log scale, the relation appears as a straight line whose slope is equal to the power $-m$ (the cementation exponent). It has been observed and widely reported that, when the range of porosities is extended (specially for small values), the data does not follow a power-law trend with a constant exponent, i.e., the lines are curved in a log-log scale, (Givens, 1987; Worthington, 1993; Padhy et al., 2006); this non-Archie behavior has been qualitatively explained by theoretical models, based on simple mixing laws (Petricola and Watfa, 1995; Fleury, 2002) or effective medium approximation (EMA) (Sen, 1997). Therefore, to obtain better predictions for the entire range of porosities and for different rock lithologies, improvements to Archie's law or new models are needed. To our knowledge, just a few attempts to model the non-constant power relation between F and Φ have appeared in the open literature (Givens, 1987; Glover et al., 2000; Bernabé et al., 2011; Nguyen, 2014).

Recently, due to the development of new software and tools in the fields of image acquisition/processing, it is possible to perform a more detailed electrical characterization of core rocks (Knackstedt et al., 2007; Elmer, 2009; Schlumberger, 2014); unfortunately, they are expensive.

In the present article we develop an expression to evaluate the formation factor, defined by Equation (1), as a function of the rock porosity and its physical properties. Our model is based on a more general study recently developed by Chávez et al. (2014), which accounted for the coupled thermo-electrical effects of a composite material to predict the electrical resistivity. Considering the range of physical properties of rocks, Chávez et al. model can be significantly simplified and an analytical expression for the formation factor is, in fact, obtained. Some comparisons between our approach and another theoretical model for the formation factor of sandstone lithologies are presented; differences and common points among both theories are pointed out. To fully validate the present model, we also conducted comparisons with experimental data for different conventional rock cores lithologies and porosities, leading to a good agreement.

The paper is organized as follows. In Section 2, we describe the mathematical formulation and the assumptions under which our problem will be set to compute the formation factor. This is followed in Section 3 with comparisons between numerical results and experimental data as well as some discussions are presented. Finally, some concluding remarks are drawn in Section 4.

2. Mathematical model

In our recent theoretical work (Chávez et al., 2014), a nonlinear conjugate thermo-electric model was developed to study the effect of frequency, resistivities and thermal conductivities on the current density and temperature profiles for a two-phase composite medium. Implementing a numerical solution in cylindrical coordinates, current density and temperature profiles were obtained for each phase. Additionally, based on Equation (1), we established an expression to evaluate the formation factor in terms of the dimensionless current densities for each phase as:

$$F = \frac{\frac{G}{\Phi}\int_0^{\sqrt{\Phi/G}} \varphi_l \xi d\xi + \frac{G}{G-\Phi}\frac{R_r}{R_l}\int_{\sqrt{\Phi/G}}^1 \varphi_r \xi d\xi}{2\left(\int_0^{\sqrt{\Phi/G}} \varphi_l \xi d\xi + \int_{\sqrt{\Phi/G}}^1 \varphi_r \xi d\xi\right)}. \tag{3}$$

where the symbols l and r stand for liquid and rock phases respectively, R is the electrical resistivity, G is the tortuosity, φ is the dimensionless electrical current density, ξ is the dimensionless radial coordinate, these last two variables are respectively defined as:

$$\xi = \frac{r^*}{b} \tag{4}$$

$$\varphi = \frac{J}{J_a} \tag{5}$$

where b is the pore-rock system radius, r^* is the dimensional radial coordinate, J and J_a are the dimensional current densities at any radius and at the pore radius, respectively.

The general model considers thermal effects on the current density distribution, through the Joule heating effect and considering the temperature-dependent resistivities of both phases. For the specific case of rocks, however, changes in temperature do not play a significant role in the calculation of F. This is, in fact, expected since the resistivity tests are commonly conducted using small currents; thus, the Joule effect becomes negligible. In this case, the equations for the current density in each phase, Equations (21) and (22) (see Appendix A), can be uncoupled from the heat conduction equation. Hence, we consider the temperature to remain constant.

In such a case, we have:

$$\frac{d^2\varphi_l}{d\xi^2} + \frac{1}{\xi}\frac{d\varphi_l}{d\xi} = \frac{2i}{\varepsilon_l^2 \Phi/G}\varphi_l, \tag{6}$$

for the liquid phase and for the rock phase:

$$\frac{d^2\varphi_r}{d\xi^2} + \frac{1}{\xi}\frac{d\varphi_r}{d\xi} = \frac{2i}{\varepsilon_r^2\left(1-\sqrt{\Phi/G}\right)^2}\varphi_r. \tag{7}$$

These equations are then subjected to the following boundary conditions:

$$\xi = 0: \quad \frac{d\varphi_l}{d\xi} = 0, \tag{8}$$

$$\xi = \sqrt{\frac{\Phi}{G}}: \quad \varphi_l = \frac{R_r}{R_l}\varphi_r, \tag{9}$$

$$\frac{\mu_r R_l}{\mu_l R_r}\frac{d\varphi_l}{d\xi} = \frac{d\varphi_r}{d\xi}, \tag{10}$$

$$\xi = 1: \quad \varphi_r = \frac{R_l}{R_r}G. \tag{11}$$

Boundary conditions given by Equation (8) through (11) represent a simplified version of Equations (23)-(26) and the are the well-known symmetry condition, the continuity of the electric field and a characteristic current density, respectively; for more details see Chávez et al. (2014).

It is worthy of note that $\Phi < 1$ and $G > 1$, therefore the RHS of Equations (6) and (7) are always finite; furthermore, they are complex and involve the ε parameter, which is defined as the ratio of the skin depth parameter δ and pore size. The skin depth is defined as $\delta = (2R/\mu\omega)^{1/2}$ where R and μ are the electric resistivity and magnetic permeability of the medium, respectively. The frequency of the electrical signal is ω. For rock cores in petroleum industry characterization, the skin depth effect becomes irrelevant since resistivity tests are usually performed using direct current or an alternating electric signal with fixed frequency of order 10^1 Hz or higher. Also the tortuosity, G, defined as in Chávez et al. (2014), is always larger or equal to one. Therefore, the terms ε_l and ε_r are of the order of 10^4 and 10^6 respectively. Consequently, the right hand side of Equations (6) and (7) are small, thus

$$\frac{d^2\varphi_l}{d\xi^2} + \frac{1}{\xi}\frac{d\varphi_l}{d\xi} = 0, \tag{12}$$

$$\frac{d^2\varphi_r}{d\xi^2} + \frac{1}{\xi}\frac{d\varphi_r}{d\xi} = 0, \tag{13}$$

This set of ordinary differential equations can be readily solved analytically considering the boundary condition given by Equations (8)-(11), the solutions for the dimensionless electrical current density in the liquid and rock phases are respectively given by:

$$\varphi_l(\xi) = G \quad 0 \le \xi \le \sqrt{\frac{\Phi}{G}}, \tag{14}$$

$$\varphi_r(\xi) = G\frac{R_l}{R_r} \quad \sqrt{\frac{\Phi}{G}} < \xi \le 1. \tag{15}$$

As can be seen, the solutions for the electrical current density in the liquid and rock phases are proportional to the tortuosity; in particular, for the rock phase the G parameter is multiplied by the ratio of the electrical resistivity of the liquid and rock, due to the higher resistivity of the rock the current density in this phase is smaller than the one in the liquid. The dependency of both solutions with G is explained by the fact that our model considers a tortuous liquid phase embedded in a cylindrical rock system (concentric circles in a cross section plane); therefore, the tortuosity parameter comes from the liquid-rock interface and from the outer surface of the rock system (Equations (9) and (11), respectively); it should be mentioned that the electrical current density distribution will depend not only on the tortuosity but also on the R_l/R_r ratio, for more details see Chávez et al. (2014).

Consequentially, with the closed expressions for both φ_l and φ_r, Equation (3) can be integrated to obtain an analytical expression for the formation factor:

$$F(\Phi) = \frac{G}{\frac{R_l}{R_r}(G-\Phi)+\Phi}. \tag{16}$$

This expression is derived from a well sustained physical model and represents an alternative to evaluate the formation factor provided that the tortuosity is known. Alternatively, knowing the formation factor (from experimental measurements), the tortuosity can be inferred. In the present work we focus our attention in the first idea.

The effect of the temperature and pressure on the electrical parameters will involve the knowledge of mathematical expressions that relate both thermodynamic variables to the electrical resistivities of rock and liquid phases; nevertheless, this is out of the scope of this paper. Furthermore, Fleury et al. (2004) reported that F does not depend significantly on the net overburden pressure even for vuggy samples and that cementation exponent values measured at ambient conditions can be used for log calibration with a reasonable accuracy. In fact, the variation of porosity and resistivity are compensating each other; yielding a quasi-constant formation factor. On the other side, F behavior as a function of the temperature, depends on the rock core lithology, for the sandstones, F decreases with temperature up to 150–175°C and then stabilizes at higher temperature, this behavior may be attributed to physical changes in pore construction because of thermal expansion (Ucok et al., 1979). In our model, the temperature effect might be included in the estimation of the resistivity value for the water saturating the core, for instance the experimental measurements reported by Xiao et al. (2013); however, the model does not take into account changes in pore construction due to thermal

expansion.

In summary, the relevant parameters to evaluate the formation factor are the resistivity ratio, R_l/R_r, which can be easily obtained from the tables or from direct measurements, the tortuosity G and the porosity Φ. Even though the model is compact and robust its usefulness depends on the knowledge of resistivity values for the rocks core, which might represent a limitation for those lithologies where the electrical characterization represents a problem (Murray and Marsden, 2009; Kumar and Hoversten, 2012).

For some of the rock lithologies different studies report the range for the R_r values; i.e., for the sedimentary rocks like sandstones $1 \leq R_r \leq 6.4 \times 10^8\ \Omega\cdot$m, for the sands $500 \leq R_r \leq 1 \times 10^4\ \Omega\cdot$m (Winkler, 1973), for the limestones $50 \leq R_r \leq 1 \times 10^7\ \Omega\cdot$m (McNeill, 1980) and for volcanic rocks $1 \leq R_r \leq 160\ \Omega\cdot$m (Shevko et al., 2013).

The tortuosity is discussed in more depth in the next section.

It is worthy of note that, for most of core lithologies $R_r \gg R_l$ which makes $\frac{R_l}{R_r} \to 0$, thus Equation (16) becomes $F = G/\Phi$, in accordance to the expression reported by Tiab and Donaldson (2004). This simple relation exhibits a simple power-law dependence of the formation factor with porosity, similar to Archie's law. On the other hand, for rock core lithologies with small R_r values, the formation factor no longer shows a constant power relation with porosity. It will be shown in the next section that this behavior is in agreement with experimental data reported in the literature.

3. Results and discussion

Before showing the results of the model, it is important to discuss the tortuosity factor; it represents complex microstructure in porous media and much affects the macroscopic transport properties characterized by parameters such as F. Literature shows that there is no clear consensus on its definition; in fact, for tortuosity estimation there are (Clennell, 1997; Ghanbarian et al., 2013): geometric models (Bo-Ming and Jian-Hua, 2004; Lanfrey et al., 2010), hydraulic models (Comiti and Renaud, 1989; Mota et al., 2001), electric models (Maxwell, 1873; Coleman and Vassilicos, 2008; Matyka and Koza, 2012), and diffusive models (Weissberg, 1963; Beeckman, 1990). All of them different in terms of their basic concepts: geometry, fluid mechanics, electrodynamics, and diffusion equation. Those models for each tortuosity are hard to be obtained from first principles analysis; however most of them are a function of Φ despite of the difference between the background concepts. Typically, an empirical model has to be used. For the results presented in this section and due to their simplicity we consider the expression proposed by Matyka and Koza (2012):

$$G = \Phi^{-\beta} \tag{17}$$

where G depends on the core lithology through the fitting parameter β, it cannot be universal, at least not without replacement of the porosity by some more general function. Conversely, if the tortuosity is known, or inferred from another method, the fitting parameter can be obtained.

It is important to emphasize that the expression for the formation factor given by Equation (16), assuming that G is given by Equation (17), predicts physically sound limiting values. For instance, as Φ tends to one, the formation factor, F also tends to one, as one would expect. For vanishing values of the porosity, we obtain that $F \to R_r/R_l$ which also makes physical sense. These limits cannot be obtained with simpler power laws, i.e., Archie's law.

The F vs. Φ behavior of the present model is analysed as a function of the β and the resistivity ratio parameters, R_l/R_r; results are shown in Fig. 1 (top and bottom, respectively). The following analysis in based on the experimental results reported by Archie (1942) for the sands core rock lithology (see Fig. 6); firstly, we started by decreasing β from 1.05 to 0.45 and fixing $R_l/R_r = 3 \times 10^{-4}$, as a result decreasing and more linear behavior for F is observed, there is a clear difference in the whole porosity range. Secondly, by increasing the resistivity ratio from 3×10^{-5} to 3×10^{-2} and now fixing $\beta = 1.05$, it is clear that at least for the three R_l/R_r smaller values, a variation of one order of magnitude for F is observed, but only for the smaller Φ values, because if $0.6 \lesssim \Phi \leq 1$ the four curves show similar results for F. The previous results would indicate that for a core rock with a given Φ value, the larger the β parameter the larger the G and F values, which makes physical sense. On the other side, for a core rock with a fixed small porosity value the larger R_r values the larger F values, this is also reconciled with physics.

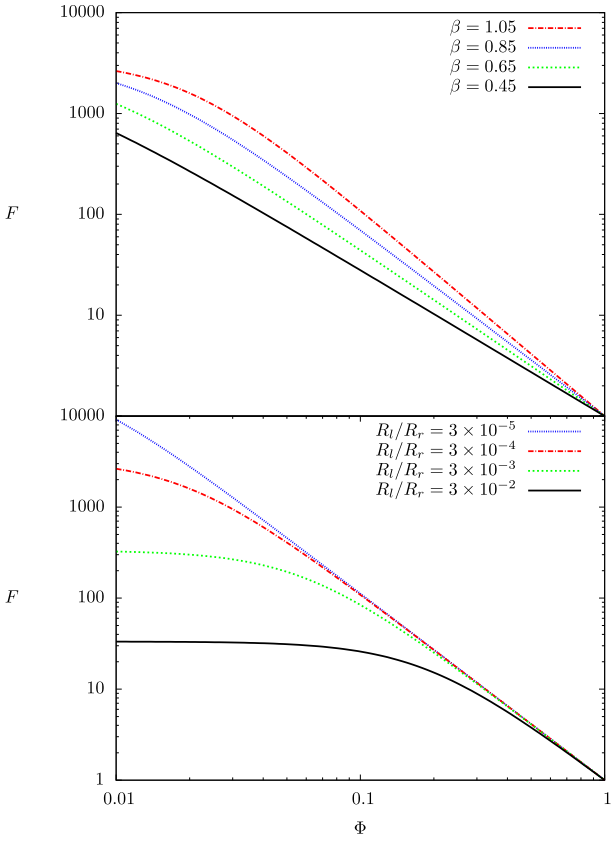

Fig. 1. Parametric studies for: the β parameter (top) using $R_l/R_r = 3 \times 10^{-4}$ and the resistivity ratio, R_l/R_r, using $\beta = 1.05$.

Recently a few models have been proposed as an alternative to Archie's law, for instance the one by Nguyen (2014) in which F is obtained numerically from a micromechanical approach to model the electrical resistivity/conductivity of sandstone assuming pore inclusions whose shape is characterized by the pore aspect ratio parameter, c; F values are obtained by numerical solution of the model. Particularly, the formation factor for compacted sandstone for the case of crack-like pores ($c = 0$) with non-conductive or conductive solids can be calculated with the following expression

$$F_{\text{Nguyen}} = \frac{\Phi \frac{R_l}{R_r} + 3 - \Phi}{(3 - 2\Phi)\frac{R_l}{R_r} + 2\Phi}, \tag{18}$$

similarly to our model, Equation (18) is a function of the resistivity ratio, R_l/R_r; it also obeys the same limiting values, as Φ tends to one, the formation factor, F also tends to one, while for vanishing values

of the porosity $F \to R_r/R_l$; so in the limits both expressions given by Equations (16) and (18) give the same values for F.

Figs. 2 and 3 show the comparisons between the numerical solution of the Nguyen's general model, some experimental data (Nguyen, 2014), and our model. It should be noted that the lines from Nguyen's model were computed for non-null values of the parameter c. At first glance, both models seem to match well to the experimental data; however it is worth noting some differences between these two approaches. Nguyen's model predicts F curves showing a non-linear growth as Φ tends to zero, this is a consequence of taking non-zero values for the fitting parameters R_l/R_r and c, which in physical terms corresponds to microcracks filled by conductive fluid that strongly reduce the electrical resistivity of rock (Nguyen, 2014). Interestingly, Nguyen found a correlation between the cementation exponent m from Archie's law and the pore aspect ratio c; in this way, he argues a physical meaning of m. The current model predicts F lines with a nearly linear growth as Φ tends to zero; in this case the fitting parameters are R_l/R_r and β.

It is important to mention that Equation (16) also satisfies the limits for the model of Voigt (1889) (upper limit) and Reuss (1929) (lower limit), commonly known as rule of mixtures, useful to predict various properties of a composite material made up of continuous and unidirectional fibres; in terms of the formation factor these limits can be read as:

$$\left(\Phi + \frac{R_l}{R_r}(1-\Phi)\right)^{-1} \leq F \leq \Phi + \frac{R_r}{R_l}(1-\Phi) \tag{19}$$

As can be seen in Fig. 4, where formation factor and upper and lower limits are plotted vs. the porosity, it is clear that Equation (16) clearly satisfies both limits for the same values of the R_l/R_r and β parameters used in Fig. 1. Both limits could be useful to determine the validity of the model for specific parameters.

Another effort for the F calculation is the one proposed by Bernabé et al. (2011); using the network simulation approach by Bernabé et al. (2010), they extended the model to include the electrical formation factor. In particular, they developed a joint permeability-formation factor model which consists of three equations and is solved via a numerical method; it does not explicitly include Φ, making difficult a direct comparison with our model. Furthermore, for the calculations, numerical values for the exponents and prefactors of the power laws of the equations are necessary. In high contrast our model is simple.

In order to continue validating our model we used physical properties for three representative sedimentary rocks present in oil reservoirs (Bassiouni, 1994): sandstone (SiO_2), sands (SiO_2) and limestone ($CaCO_3$); additionally, comparisons with data from volcanic rocks were also performed; G values for sedimentary rocks were obtained from the literature (Frosch et al., 2000; Wang et al., 2005); while the ones for volcanic are fixed in order to get the best fit with our model. Furthermore, based on power law nature of Archie's law, a cementation exponent m_A can be deduced as:

$$m_A = -\frac{ln(F)}{ln(\Phi)}. \tag{20}$$

Considering this equation it is possible to calculate the cementation exponent for different values of Φ if F is obtained from Equation (16). In this manner, the average cementation exponent, m_t, can be calculated for a given range of porosities. If the data is closely represented by Archie's law then $m_t \approx m_A$. If these values are not close, then Archie's law will fail to model the data, at least for the given porosity range.

Firstly, we performed comparisons with experimental data for sandstone and sands rock core lithologies, in particular with the data from Archie (1942), who measured the resistivity of the rock saturated with brine and determined F for a variety of sandstones

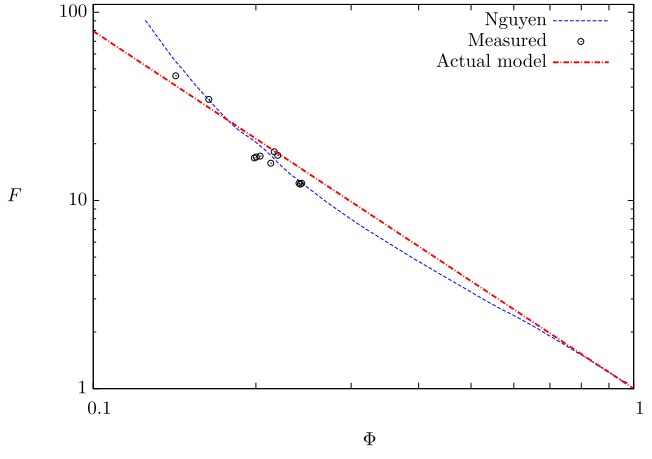

Fig. 2. Comparison between numerical values for F and experimental data for rocks core with a sandstone lithology, both reported by Nguyen (2014); and the present model for which $\beta = 0.9$, $R_l = 0.1\ \Omega\cdot$m and $R_r = 10000\ \Omega\cdot$m values were used.

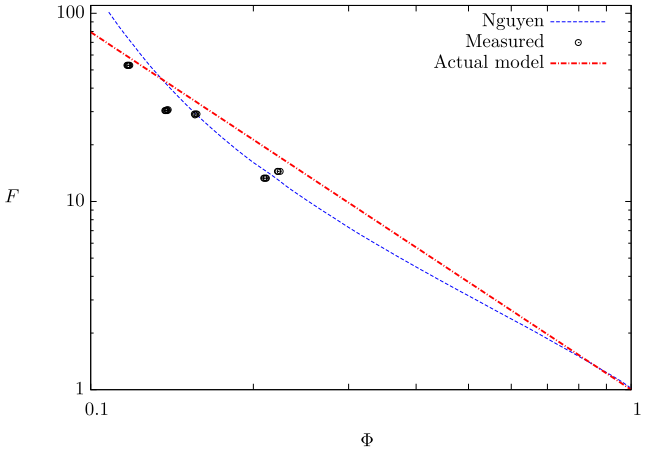

Fig. 3. Comparison between numerical values for F and experimental data for rocks core with a sandstone lithology, both reported by Nguyen (2014); and the present model for which $\beta = 0.9$, $R_l = 0.1\ \Omega\cdot$m and $R_r = 10000\ \Omega\cdot$m values were used.

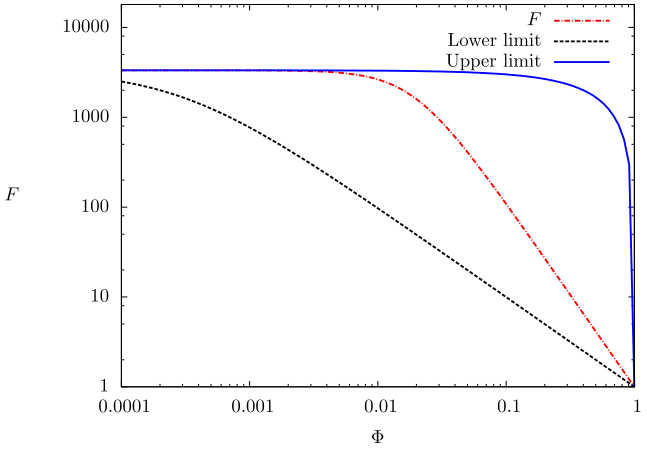

Fig. 4. Comparison between the limits for the model of Voigt (1889) (upper limit) and Reuss (1929) (lower limit) and the present model for which the $R_l/R_r = 3 \times 10^{-4}$ and $\beta = 1.05$ values were used.

from the Gulf of the United States. Fig. 5 shows the comparison between experimental data and Equation (16) for the formation factor. Reported values for the cementation exponent m_A by Archie are in the range of 1.8–2. Clearly, our model fits the data well.

Archie (1942) also reported measurements for rocks core of a sand lithology type. A comparison between his measurements and our model is shown in Fig. 6. G values were obtained from (Guillon et al., 1998). In this case the comparison between experiments and predictions from the model agree well. Note that porosity values for both, sandstone and sands core rock lithologies reported by Archie are in the range between 0.1 and 0.4. The measured formation factor matches well with the analytic expression, which for this range of porosity values exhibits a constant m power-law behavior.

More recently, experimental data for the formation factor for sandstone rock core lithologies have been reported (Xiao et al., 2013). Figs. 7–9 show a comparison between their experimental results and model predictions. The comparison is, again, good for the entire porosity range. In this case, the porosity values are in the range of 0.04–0.2, smaller than those reported by Archie (1942). For such a range of porosities the data does not follow the constant cementation exponent behavior of Archie's law. The prediction of our model, on the other hand, readily captures this behavior.

Additionally, we also present comparisons with experimental data for the volcanic lithologies, whose main characteristic is that they tend to be extremely hard compared to sedimentary rocks. Volcanic rocks have been ignored by the petroleum industry because of a perceived lack of reservoir quality (Farooqui et al., 2009). Recently, using the electrical resistivity tomography method values for F have been reported by Shevko et al. (2013). Figs. 10 and 11 show comparisons between our model for F and experimental data for andesite and andesidacites (volcanic rocks), respectively.

As a final test to assess the validity of the model presented here, we compare the predictions of Equation (16) with our own experimental data. Two different kind of rock cores (sandstone and limestone) were extracted from two sites in Mexico, located near the coast of the Gulf of Mexico. The cores were then sent to Core Laboratories Inc. for a complete characterization. The protocol followed to obtain the formation factor can be found in CORE Laboratories (2012). Figs. 12 and 13 show comparisons of the data

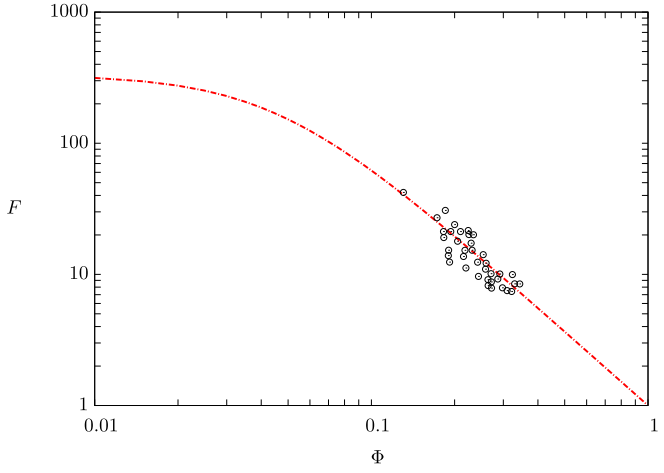

Fig. 5. Comparison between analytic expression for F and experimental data for rocks core with a sandstone lithology reported by Archie (1942), where the theoretical cementation exponent is $m_t = 1.88$ and the experimental one is $m_A = 1.8 - 2.0$, for the analytic calculation, values for $\beta = 0.88$, $R_l = 0.3\ \Omega\cdot$m and $R_r = 100\ \Omega\cdot$m were used.

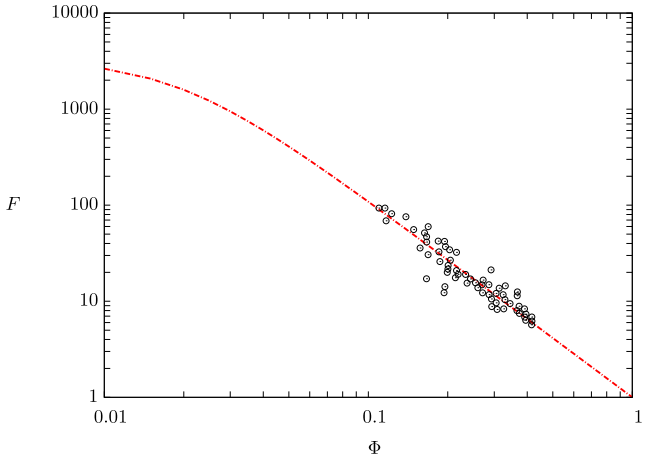

Fig. 6. Comparison between analytic expression for F and experimental data for rocks core with a sands lithology reported by Archie (1942), where the theoretical cementation exponent is $m_t = 2.0$ and the experimental one is $m_A = 1.93$, for the analytic calculation, values for $\beta = 1.05$, $R_l = 0.3\ \Omega\cdot$m and $R_r = 1000\ \Omega\cdot$m were used.

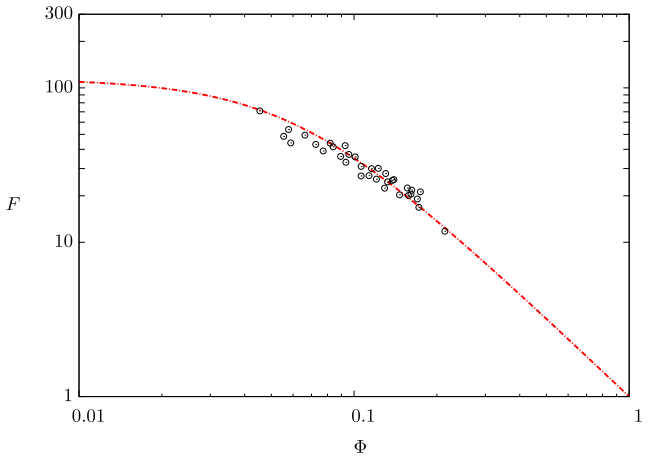

Fig. 7. Comparison between analytic expression for F and experimental data for rocks core with a sandstone lithology reported by Xiao et al. (2013), where the theoretical cementation exponent is $m_t = 1.57$ and the experimental one is $m_A = 1.24$, for the analytic calculation, values for $\beta = 0.7$, $R_l = 0.07\ \Omega\cdot$m and $R_r = 8\ \Omega\cdot$m were used.

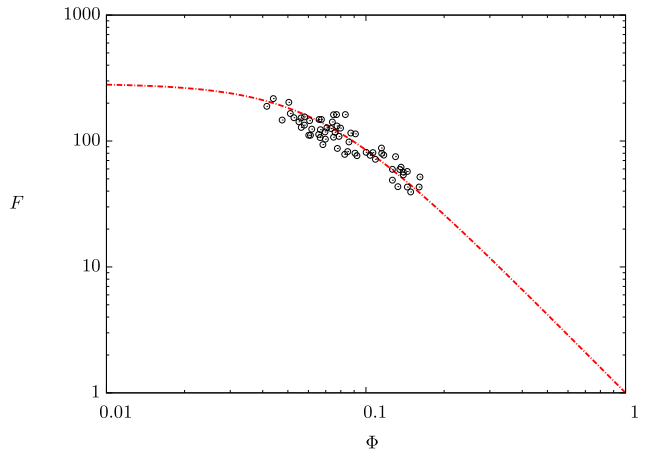

Fig. 8. Comparison between analytic expression for F and experimental data for rocks core with a sandstone lithology reported by Xiao et al. (2013), where the theoretical cementation exponent is $m_t = 1.91$ and the experimental one is $m_A = 1.60$, for the analytic calculation, values for $\beta = 1.08$, $R_l = 0.07\ \Omega\cdot$m and $R_r = 20\ \Omega\cdot$m were used.

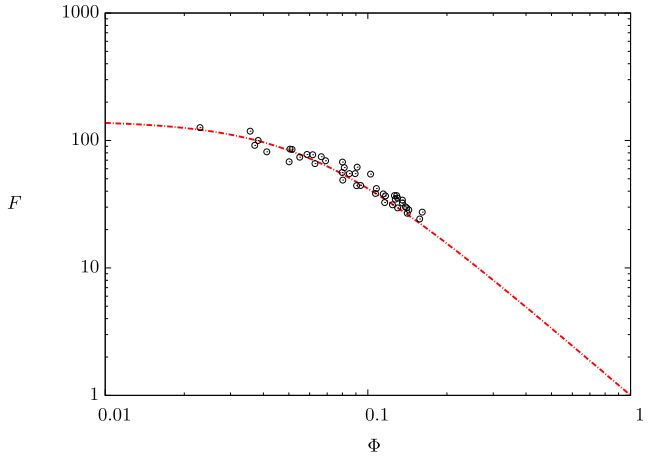

Fig. 9. Comparison between analytic expression for F and experimental data for rocks core with a sandstone lithology reported by Xiao et al. (2013), where the theorical cementation exponent is $m_t = 1.56$ and the experimental one is $m_A = 1.16$, for the analytic calculation, values for $\beta = 0.77$, $R_l = 0.07\ \Omega{\cdot}$m and $R_r = 10\ \Omega{\cdot}$m were used.

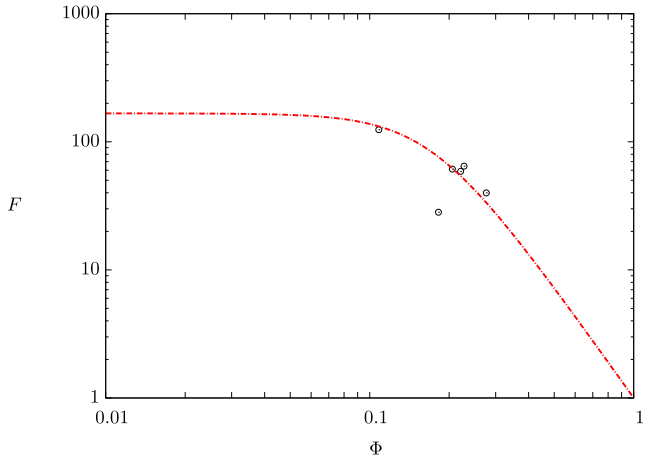

Fig. 10. Comparison between analytic expression for F and experimental data for rocks core with an andesite lithology reported by Shevko et al. (2013), where the theorical cementation exponent is $m_t = 2.58$ and the experimental one is $m_A = 2.19$, for the analytic calculation, values for $\beta = 1.9$, $R_l = 0.9\ \Omega{\cdot}$m and $R_r = 150\ \Omega{\cdot}$m were used.

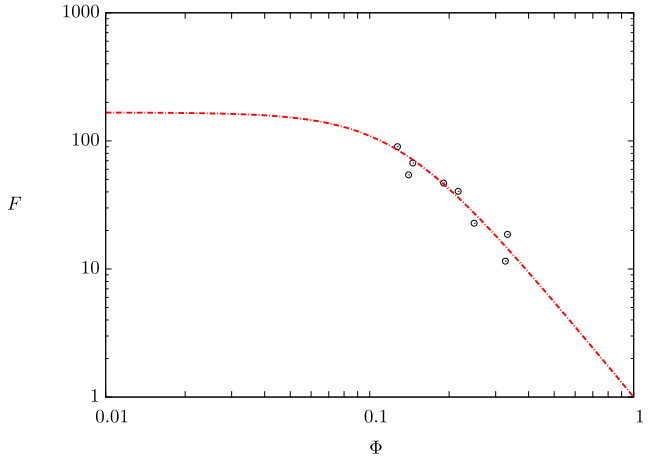

Fig. 11. Comparison between analytic expression for F and experimental data for rocks core with an andesidacites lithology reported by Shevko et al. (2013), where the theorical cementation exponent is $m_t = 2.33$ and the experimental one is $m_A = 2.11$, for the analytic calculation, values for $\beta = 1.5$, $R_l = 0.9\ \Omega{\cdot}$m and $R_r = 150\ \Omega{\cdot}$m were used.

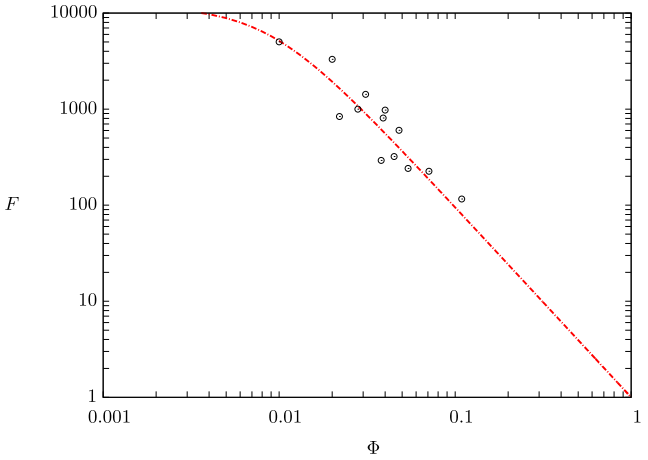

Fig. 12. Comparison between analytic expression for F and experimental data for rocks core with a sandstone lithology reported by CORELAB, where the theorical cementation exponent is $m_t = 1.98$ and the experimental one is $m_A = 1.96$, for the analytic calculation, values for $\beta = 0.98$, $R_l = 0.085\ \Omega{\cdot}$m and $R_r = 1000\ \Omega{\cdot}$m were used.

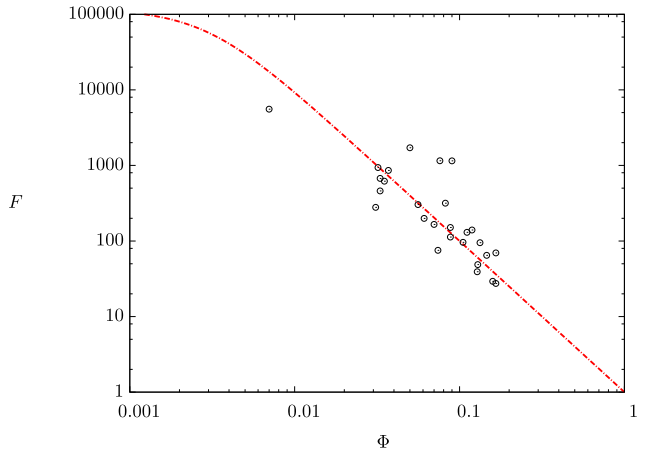

Fig. 13. Comparison between analytic expression for F and experimental data for rocks core with a limestone lithology reported by CORELAB, where the theorical cementation exponent is $m_t = 2.0$ and the experimental one is $m_A = 2.0$, for the analytic calculation, values for $\beta = 1.0$, $R_l = 0.085\ \Omega{\cdot}m$ and $R_r = 10000\ \Omega{\cdot}$m were used.

with model predictions for the cases of sandstone and limestone lithologies, respectively. The values of G were obtained from Dolch (1959); Wang et al. (2005). It can be noticed that although the porosity range for these samples is smaller than that in Fig. 5, the formation factor does show the constant m behavior. Clearly, in this case the predictions of the model fit the data very well, despite the changes in porosity and different petrophysical properties.

As can be seen in Fig. 13, experimental data are quite dispersed; anyway, we performed comparisons with other experimental data for the limestone lithology reported by Widarsono (2011) and also a good agreement is found, for instance see Figs. 14 and 15.

The previous results show that depending on the porosity range and on the physical properties of the core (specifically the value of R_l/R_r), the formation factor can exhibit two different behaviors. A single constant-m power law is observed for large porosities ($0.2 < \Phi < 0.5$) and small values of R_l/R_r. On the other hand, the formation factor does not follow a constant m-power behavior when the porosity is smaller ($0.001 < \Phi < 0.2$) and the ratio R_l/R_r is large.

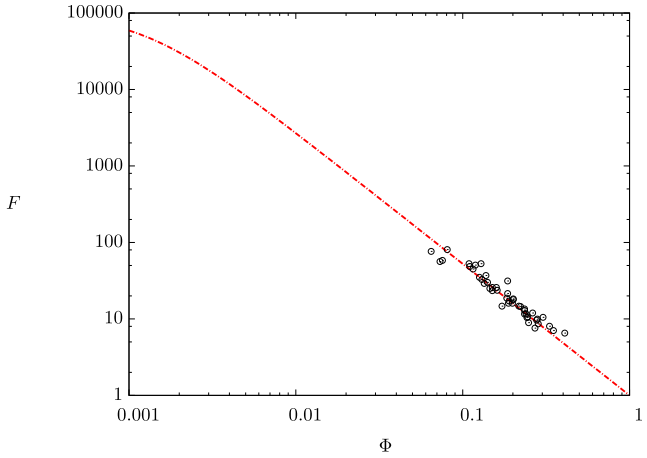

Fig. 14. Comparison between analytic expression for F and experimental data for rocks core with a limestone lithology reported by Widarsono (2011), where the theorical cementation exponent is $m_t = 1.72$ and the experimental one is $m_A = 1.76$., for the analytic calculation, values for $\beta = 0.72$, $R_l = 0.1\ \Omega{\cdot}\text{m}$ and $R_r = 10000\ \Omega{\cdot}\text{m}$ were used.

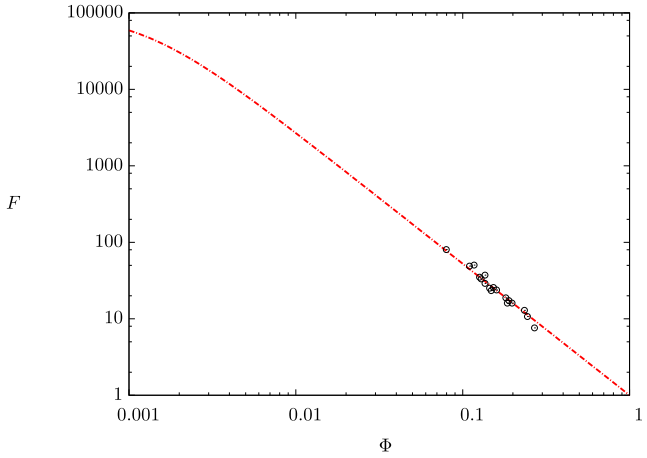

Fig. 15. Comparison between analytic expression for F and experimental data for rocks core with a limestone lithology reported by Widarsono (2011), where the theorical cementation exponent is $m_t = 1.72$ and the experimental one is $m_A = 1.73$, for the analytic calculation, values for $\beta = 0.72$, $R_l = 0.1\ \Omega{\cdot}\text{m}$ and $R_r = 10000\ \Omega{\cdot}\text{m}$ were used.

Hence, both porosity and R_l/R_r need to be known to determine the change of the formation factor with porosity. Our model reproduce very well experimental data for the four different lithologies previously shown.

4. Conclusions

We derived an analytical expression for the formation factor based on physical principles. The predictions of our model were validated by comparing with experimental data that considered different ranges of porosity and different rock lithologies. The formation factor can be calculated directly if the resistivity ratio, R_l/R_r, the tortuosity G and the porosity Φ are known. Results for different rock core lithologies are shown and validated. Our model is capable of reproducing the different trends observed in experimental data and compares well with other expressions for F. The implementation of the expression proposed here is simple and robust. This new model could also be extended to attempt to predict the electrical conductivity of more complex materials; for instance, the shape of pore inclusions or even microcracks filled by conductive fluid. Furthermore, it could be useful to infer the tortuosity for core samples whose formation factor values are obtained from experimental measurements. We plan to explore these ideas in the future.

Acknowledgments

A. Beltrán thanks UNAM-DGAPA-PAPIIT for support under Project No. IA102315. We also thank two anonymous reviewers for their constructive comments, which helped us to improve the manuscript.

Appendix A

In this section we present the information to derive the proposed model for the dimensionless electrical current density, φ, given by Equations (6) and (7) and the respective boundary conditions, Equations (14)-(15); for more details see Chávez et al. (2014).

The propagation of a dimensionless electrical current density in a composite medium of two non-deformable phases depicted schematically in Fig. 16, allow us to evaluate the formation factor, Equation (3), by solving the following equations for the:

Internal phase model:

$$\frac{d^2\varphi_l}{d\xi^2} + \left(2\frac{\kappa_l}{(1+\kappa_l\theta_l)}\frac{\partial\theta_l}{\partial\xi} + \frac{1}{\xi}\right)\frac{d\varphi_l}{d\xi} + \frac{\kappa_l}{1+\kappa_l\theta_l}\left(\frac{\partial^2\theta_l}{\partial\xi^2} + \frac{1}{\xi}\frac{\partial\theta_l}{\partial\xi}\right)\varphi_l = \frac{2i}{(1+\kappa_l\theta_l)\varepsilon_l^2\Phi/G}\varphi_l, \tag{21}$$

and external phase model:

$$\frac{d^2\varphi_r}{d\xi^2} + \left(2\frac{\kappa_r}{(1+\kappa_r\theta_r)}\frac{\partial\theta_r}{\partial\xi} + \frac{1}{\xi}\right)\frac{d\varphi_r}{d\xi} + \frac{\kappa_r}{1+\kappa_r\theta_r}\left(\frac{\partial^2\theta_r}{\partial\xi^2} + \frac{1}{\xi}\frac{\partial\theta_r}{\partial\xi}\right)\varphi_r = \frac{2i}{(1+\kappa_r\theta_r)\varepsilon_r^2\left(1-\sqrt{\Phi/G}\right)^2}\varphi_r, \tag{22}$$

with their boundary conditions:

$$\xi = 0: \quad \frac{d\varphi_l}{d\xi} = 0, \tag{23}$$

$$\xi = \sqrt{\frac{\Phi}{G}}: \varphi_l = \frac{R_r[1+\kappa_r\theta_r]}{R_l[1+\kappa_l\theta_l]}\varphi_r, \tag{24}$$

$$\frac{\mu_r R_l}{\mu_l R_r}\frac{(1+\kappa_l\theta_l)}{(1+\kappa_r\theta_r)}\left(\frac{d\varphi_l}{d\xi} + \frac{\kappa_l}{1+\kappa_l\theta_l}\frac{\partial\theta_l}{\partial\xi}\varphi_l\right) = \left(\frac{d\varphi_r}{d\xi} + \frac{\kappa_r}{1+\kappa_r\theta_r}\frac{\partial\theta_r}{\partial\xi}\varphi_r\right), \tag{25}$$

$$\xi = 1: \quad \varphi_r = \frac{R_l}{R_r}G. \tag{26}$$

where $\kappa_{l,r} = \phi_{l,r}\Delta T_c$, ϕ is the temperature coefficient for resistivity, ΔT_c is a characteristic temperature drop and θ is the dimensionless temperature.

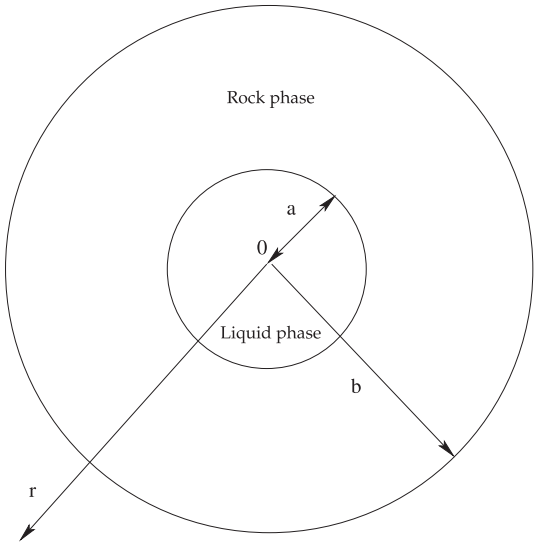

Fig. 16. Schematic representation of the composite medium under study.

References

Archie, G.E., 1942. The electrical resistivity log as an aid in determining some reservoir characteristics. Trans. AIME 146.

Bassiouni, Z., 1994. Theory, Measurement, and Interpretation of Well Logs. SPE Textbook Series. Henry L. Doherty Memorial Fund of AIME, Society of Petroleum Engineers, Richardson (Tex.). URL. http://opac.inria.fr/record=b1100909.

Beeckman, J., 1990. Mathematical description of heterogeneous materials. Chem. Eng. Sci. 45 (8), 2603–2610.

Bernabé, Y., Li, M., Maineult, A., 2010. Permeability and pore connectivity: a new model based on network simulations. J. Geophys. Res. Solid Earth 115 (B10), b10203. http://dx.doi.org/10.1029/2010JB007444 n/a–n/a.

Bernabé, Y., Zamora, M., Li, M., Maineult, A., Tang, Y.B., 2011. Pore connectivity, permeability, and electrical formation factor: a new model and comparison to experimental data. J. Geophys. Res. Solid Earth 116 (B11), b11204. http://dx.doi.org/10.1029/2011JB008543 n/a–n/a.

Bo-Ming, Y., Jian-Hua, L., 2004. A geometry model for tortuosity of flow path in porous media. Chin. Phys. Lett. 21 (8), 1569. URL. http://stacks.iop.org/0256-307X/21/i=8/a=044.

Chávez, O., Godínez, F.A., Beltrán, A., García, A., Zenit, R., 05 2014. A conjugate thermo-electric model for a composite medium. PLoS ONE 9 (5), 1–10. Doi: 10.1371%2Fjournal.pone.0097895.

Clavier, C., Coates, G., Dumanoir, J., 1977. Theoretical and experimental bases for the dual-water model for interpretation of shaly sands. SPE J. 24 (2), 153–168.

Clennell, M.B., 1997. Tortuosity: a guide through the maze. Geol. Soc. Lond. Spec. Publ. 122 (1), 299–344.

Coleman, S.W., Vassilicos, J.C., Jan 2008. Transport properties of saturated and unsaturated porous fractal materials. Phys. Rev. Lett. 100 (035504) http://dx.doi.org/10.1103/PhysRevLett.100.035504.

Comiti, J., Renaud, M., 1989. A new model for determining mean structure parameters of fixed beds from pressure drop measurements: application to beds packed with parallelepipedal particles. Chem. Eng. Sci. 44 (7), 1539–1545. URL. http://www.sciencedirect.com/science/article/pii/0009250989800314.

CORE Laboratories, 2012. Análisis especiales de núcleo. tech. rep. hou-120483 (TEMPLE, S. A. de C. V).

Dolch, W.L., 1959. Studies of Limestone Aggregates by Fluid-flow Methods : Technical Paper. Joint Highway Research Project. Indiana Department of Transportation and Purdue University, West Lafayette. Indiana Publication FHWA/IN/JHRP-59/15.

Egbai, J.C., Aigbogun, C.O., 2012. Mathematical modelling of petrophysical parameters for reservoir characterization using well log data. Adv. Appl. Sci. Res. 3 (2), 656.

Elmer, J.B., 2009. 3D nano-scale imaging and computing of reservoir rock properties and fluid flow. Scand. Oil-Gas Mag. 5 (6).

Farooqui, M.Y., Hou, H., Li, G., Machin, N., Neville, T., Pal, A., Shrivastva, C., Wang, Y., Yang, F., Yin, C., Zhao, J., Yang, X., 2009. Evaluating volcanic reservoirs. Oilfield Rev. 21 (1).

Fleury, M., 2002. Resistivity in carbonates: new insights. In: Proceedings of the Annual Symposium of the Society of Core Analysts SCA2002-28.

Fleury, M., Efnik, M., Kalam, M., 2004. Evaluation of water saturation from resistivity in a carbonate field. from laboratory to logs. Int. Symp. Soc. Core Anal. 22, 1–12.

Frosch, G.P., Tillich, J.E., Haselmeier, R., Holz, M., Althaus, E., 2000. Probing the pore space of geothermal reservoir sandstones by nuclear magnetic resonance. Geothermics 29 (6), 671–687. URL. http://www.sciencedirect.com/science/article/pii/S0375650500000316.

Ghanbarian, B., Hunt, A.G., Ewing, R.P., Sahimi, M., 2013. Tortuosity in porous media: a critical review. Soil Sci. Soc. Am. J. 77 (5), 1461–1477.

Givens, W.W., 1987. A conductive rock matrix model (crmm) for the analysis of low-contrast resistivity formations. Soc. Petrophys. Well-Log Analysts 28 (2), 138–151.

Glover, P.W.J., Hole, M.J., Pous, J., 2000. A modified archives law for two conducting phases. Earth Planet. Sci. Lett. 180 (34), 369–383. URL. http://www.sciencedirect.com/science/article/pii/S0012821X00001680.

Guillon, L., Moussatov, A., Brouard, B., Ayrault, C., 1998. Propagation of sound in sands: measurements and modeling. In: OCEANS '98 Conference Proceedings, vol. 1, pp. 380–384.

Knackstedt, M.A., Arns, C.H., Sheppard, A.P., Senden, T.J., Sok, R.M., Cinar, Y., Olafuyi, A.O., Pinczewski, W.V., Padhy, G., Ioannidis, M., 2007. Pore scale analysis of electrical resistivity in complex core material. Int. Symp. Soc. Core Anal. 33.

Kumar, D., Hoversten, G., 2012. Geophysical model response in a shale gas. Geohorizons 17 (1), 31–37.

Lanfrey, P.Y., Kuzeljevic, Z.V., Dudukovic, M.P., 2010. Tortuosity model for fixed beds randomly packed with identical particles. Chem. Eng. Sci. 65 (5), 1891–1896. URL. http://www.sciencedirect.com/science/article/pii/S0009250909008045.

Matyka, M., Koza, Z., 2012. How to calculate tortuosity easily? AIP Conf. Proc. 1453 (1), 17–22. URL. http://scitation.aip.org/content/aip/proceeding/aipcp/10.1063/1.4711147.

Maxwell, J.C., 1873. A Treatise on Electricity and Magnetism, vol. 1. Clarendon Press, London.

McNeill, J.D., 1980. Electrical conductivity of soils and rocks. Geonics Ltd. Tec. Note TN-5 20.

Mota, M., Teixeira, J.A., Bowen, W.R., Yelshin, A., 2001. Binary spherical particle mixed beds : porosity and permeability relationship measurement. Trans. Filtr. Soc. 44, 101–106.

Murray, D., Marsden, S., 2009. Formation resistivity evaluation in tight gas sands in China. In: Second SPWLA-India Symposium.

Nguyen, S., 2014. Micromechanical approach for electrical resistivity and conductivity of sandstone. J. Appl. Geophys. 111, 135–140. URL. http://www.sciencedirect.com/science/article/pii/S0926985114002870.

Padhy, G.S., Ioannidis, M.A., Lemaire, C., Coniglio, M., 2006. Measurement and interpretation of non-archie resistivity behavior in model and real vuggy carbonates. Int. Symp. Soc. Core Anal.

Pérez-Rosales, C., 1982. On the Relationship between Formation Resistivity Factor and Porosity. Society of Petroleum Engineers 22(4).

Petricola, M., Watfa, M., 1995. Effect of microporosity in carbonates: introduction of a versatile saturation equation. SPE Middle East. Oil Show. 28841, 607–615.

Reuss, A., 1929. Berechnung der fliegrenze von mischkristallen auf grund der plastizittsbedingung fr einkristalle. ZAMM - J. Appl. Math. Mech./Zeitschrift fr Angewandte Math. und Mech. 9 (1), 49–58. http://dx.doi.org/10.1002/zamm.19290090104.

Saner, S., Al-Harthi, A., Htay, M.T., 1996. Use of tortuosity for discriminating electrofacies to interpret the electrical parameters of carbonate reservoir rocks. J. Petroleum Sci. Eng. 16 (4), 237–249. URL. http://www.sciencedirect.com/science/article/pii/S0920410596000459.

Schlumberger, 2014. Reservoir Laboratory. URL. http://www.slb.com/labs.

Sen, P.N., 1997. Resistivity of partially saturated carbonate rocks with microporosity. Geophysics 62 (2), 415–425.

Sheriff, R.E., 1974. Encyclopedic Dictionary of Exploration Geophysics, 2nd. Edition. Society of Exploration Geophysicists, Tulsa, Oklahoma.

Shevko, A.Y., Gora, M.P., Golikov, N.A., Panin, G.L., Bessonova, E.P., 2013. Using petrophysical properties of volcanic rocks in the interpretation of geophysical data (volcano ebeko, kuril islands). Open J. Geol. 3 (2B).

Tiab, D., Donaldson, E.C., 2004. Petrophysics, 2nd. Edition. Elsevier, USA.

Ucok, H., Ershaghi, I., Olhoeft, G.R., Handy, L.L., 1979. Resistivity of Brine Saturated Rock Samples at Elevated Temperatures. Stanford Geothermal Workshop.

Voigt, W., 1889. Ueber die Beziehung zwischen den beiden Elasticitätsconstanten isotroper Körper. Ann. Phys. 274, 573–587.

Wang, R., Pavlin, T., Rosen, M.S., Mair, R.W., Cory, D.G., Walsworth, R.L., 2005. Xenon NMR measurements of permeability and tortuosity in reservoir rocks. Magn. Reson. Imaging 23.

Waxman, M., 1974. Electrical conductivities in shaly sands: (i) the relation between hydrocarbon saturation and resistivity index; (ii) the temperature coefficient of electrical conductivity. J. Pet. Technol. 26 (3), 213–225.

Waxman, M., Smits, L., 1968. Ionic double-layer conductivity in oil-bearing shaly sands. SPE Form. 4 (1), 20–32.

Weissberg, H.L., 1963. Effective diffusion coefficient in porous media. J. Appl. Phys. 34 (9), 2636–2639. URL. http://scitation.aip.org/content/aip/journal/jap/34/9/10.1063/1.1729783.

Widarsono, B., 2011. The importance of litho-facies distinction in determining the most representative cementation factors for well-log evaluation: an old issue persistently neglected. Sci. Contrib. oil gas 34.

Winkler, E.M., 1973. Stone Properties, Durability in Mans Environment, first ed. Springer Verlag, New York.

Worthington, P.F., 1993. The uses and abuses of the archie equations, 1: the formation factor-porosity relationship. J. Appl. Geophys. 30 (3), 215–228. URL.

http://www.sciencedirect.com/science/article/pii/092698519390028W.
Xiao, L., Zou, C., Mao, Z., Shi, Y., Liu, X., Jin, Y., Guo, H., Hu, X., 2013. Estimation of water saturation from nuclear magnetic resonance (NMR) and conventional logs in low permeability sandstone reservoirs. J. Petroleum Sci. Eng. 108, 40–51. URL. http://www.sciencedirect.com/science/article/pii/S0920410513001502.
Yan, J., 2002. Reservoir parameters estimation from well log and core data: a case study from the north sea. Pet. Geosci. 8, 63–69.